Am J Nucl Med Mol Imaging 2014;4(1):1-9
www.ajnmmi.us /ISSN:2160-8407/ajnmmi1310005

Original Article

Positron emission tomography imaging of CD105 expression in a rat myocardial infarction model with ^{64}Cu-NOTA-TRC105

Hakan Orbay[1], Yin Zhang[2], Hector F Valdovinos[2], Guoqing Song[3], Reinier Hernandez[2], Charles P Theuer[4], Timothy A Hacker[3], Robert J Nickles[2], Weibo Cai[1,2,5]

[1]Department of Radiology, University of Wisconsin - Madison, WI, USA; [2]Department of Medical Physics, University of Wisconsin - Madison, WI, USA; [3]Department of Medicine, Division of Cardiovascular Medicine, University of Wisconsin - Madison, WI, USA; [4]TRACON Pharmaceuticals, Inc., San Diego, CA, USA; [5]University of Wisconsin Carbone Cancer Center, Madison, WI, USA

Received October 26, 2013; Accepted November 17, 2013; Epub December 15, 2013; Published January 1, 2014

Abstract: Biological changes following myocardial infarction (MI) lead to increased secretion of angiogenic factors that subsequently stimulate the formation of new blood vessels as a compensatory mechanism to reverse ischemia. The goal of this study was to assess the role of CD105 expression during MI-induced angiogenesis by positron emission tomography (PET) imaging using ^{64}Cu-labeled TRC105, an anti-CD105 monoclonal antibody. MI was induced by ligation of the left anterior descending (LAD) artery in female rats. Echocardiography and ^{18}F-fluoro-2-deoxy-D-glucose (^{18}F-FDG) PET scans were performed on post-operative day 3 to confirm the presence of MI in the infarct group and intact heart in the sham group, respectively. Ischemia-induced angiogenesis was non-invasively monitored with ^{64}Cu-NOTA-TRC105 (an extensively validated PET tracer in our previous studies) PET on post-operative days 3, 10, and 17. Tracer uptake in the infarct zone was highest on day 3 following MI, which was significantly higher than that in the sham group (1.41 ± 0.45 %ID/g vs 0.57 ± 0.07 %ID/g; n=3, $p<0.05$). Subsequently, tracer uptake in the infarct zone decreased over time to the background level on day 17, whereas tracer uptake in the heart of sham rats remained low at all time points examined. Histopathology documented increased CD105 expression following MI, which corroborated in vivo findings. This study indicated that PET imaging of CD105 can be a useful tool for MI-related research, which can potentially improve MI patient management in the future upon clinical translation of the optimized PET tracers.

Keywords: Angiogenesis, myocardial infarction (MI), positron emission tomography (PET), CD105 (endoglin), molecular imaging, ^{64}Cu

Introduction

Myocardial infarction (MI), one of the most significant consequences of coronary artery disease (CAD), remains the leading cause of death in the United States despite the decreasing trend over the last several decades [1]. After MI, a complex biological process that involves inflammation, angiogenesis, and repair can lead to ventricular remodeling, which is characterized by specific biochemical and structural alterations in the myocardial infarct and peri-infarct regions [2]. Angiogenesis represents the formation of new capillaries by cellular outgrowth from existing microvessels, which plays a critical role in the response to ischemia associated with MI [2, 3]. Non-invasive imaging of angiogenesis (e.g., its presence, extent, and time course) is an attractive strategy to improve post-infarction risk stratification and possibly guide therapeutic interventions [3, 4].

Currently, most of the information regarding the biologic pathways involved in remodeling after MI derives from ex vivo tissue analysis, whereas molecular imaging techniques can enable the monitoring of biological changes during a disease process even before the symptoms are present [5, 6]. Positron emission tomography (PET) imaging is increasingly being investigated and utilized for early detection of CAD and the evaluation of myocardial viability after MI, since

it can offer several technical advantages over other molecular imaging modalities such as higher sensitivity and quantitation accuracy [5, 7].

Vascular endothelial growth factor receptor (VEGFR) and integrins (particularly the $\alpha_v\beta_3$ integrin) have been identified as suitable targets for imaging of angiogenesis [8, 9], and several tracers targeting these receptors have been investigated in MI models [10-13]. To better define the factors that may be involved in ischemia induced-angiogenesis, we have developed a series of PET probes that bind to CD105 (endoglin), a 180 kDa disulfide-linked homodimeric transmembrane protein selectively expressed on the endothelial cells of newly formed vessels [14-17]. These tracers were all based on TRC105, a chimeric monoclonal antibody that binds to human and murine CD105 with high avidity. TRC105 has been studied as an anti-angiogenic agent in multiple clinical trials in oncology patients [18].

In this study, we evaluated the use of ^{64}Cu-NOTA-TRC105 (NOTA denotes 1,4,7-triazacyclononane-1,4,7-triacetic acid) for non-invasive and quantitative monitoring of CD105 expression in a rat model of MI using PET. We hypothesized that CD105 plays an important role during the remodeling process after MI, which could be non-invasively visualized with PET and potentially be useful for guiding future therapeutic intervention.

Materials and methods

^{64}Cu-labeling of TRC105

TRC105 was provided by TRACON Pharmaceuticals, Inc. (San Diego, CA) and S-2-(4-isothiocyanatobenzyl)-NOTA (abbreviated as p-SCN-Bn-NOTA) was purchased from Macrocyclics, Inc. (Dallas, TX). ^{64}Cu was produced with a CTI RDS 112 cyclotron using the ^{64}Ni (p, n) ^{64}Cu reaction, which has specific activity of >5 Ci/μmol at the end-of-bombardment. ^{64}Cu-NOTA-TRC105 was synthesized and comprehensively characterized both in vitro and in vivo (e.g. tumor models and murine hindlimb ischemia model), as described in detail in our previous studies [19, 20]. In brief, NOTA conjugation was carried out at pH 9.0, with the ratio of p-SCN-Bn-NOTA: TRC105 being 25:1. NOTA-TRC105 was purified using PD-10 columns (GE Healthcare, Buckinghamshire, UK) with phosphate-buffered saline (PBS, HyClone laboratories, Logan, UT) as the mobile phase. For radiolabeling, $^{64}CuCl_2$ (74 MBq) was diluted in 300 μL of 0.1 M sodium acetate buffer (pH 6.5) and added to 50 μg of NOTA-TRC105. The reaction mixture was incubated for 30 min at 37°C with constant shaking. ^{64}Cu-NOTA-TRC105 was purified using PD-10 columns with PBS as the mobile phase. The radioactive fractions containing ^{64}Cu-NOTA-TRC105 were collected and passed through a 0.2 μm syringe filter for in vivo experiments.

Rat model of MI

All animal studies were conducted under a protocol approved by the University of Wisconsin Institutional Animal Care and Use Committee. Adult female rats (200-250 g) were divided into two study groups: sham-operated control (n=3) and MI (n=3). Anesthesia was maintained with 2% isoflurane during surgery. Animals were intubated and ventilated using a small animal ventilator (Harvard Apparatus, March-Hugstetten, Germany) at 60 breaths/min with a tidal volume of 2 ml. The anterior and lateral abdominal walls were trichotomized and disinfected with iodopovidone solution prior to the incision. A transverse skin incision was performed in the upper abdominal region below the xyphoid process and a skin flap was elevated up to the second intercostal space, thereby exposing the left thoracic wall. A left thoracotomy incision was performed through the muscle layer at the fourth intercostal space level, and the left anterior descending (LAD) artery was ligated immediately after it emerged past the tip of the left atria using 6.0 nylon suture with a tapered needle (AROSurgical Corp., Newport Beach, CA). Blanching of the tissue distal to the suture was observed in all rats in the MI group. For the sham operation, suture was passed through the cardiac ventricular wall as described above but no knot was placed. The lungs were re-expanded and chest wall and skin incisions were closed separately. The animals were removed from the ventilator and allowed to recover.

Transthoracic echocardiography and PET confirmation of MI

MI was confirmed by using a Vevo 770 ultrasound system with a 17.5 MHz transducer

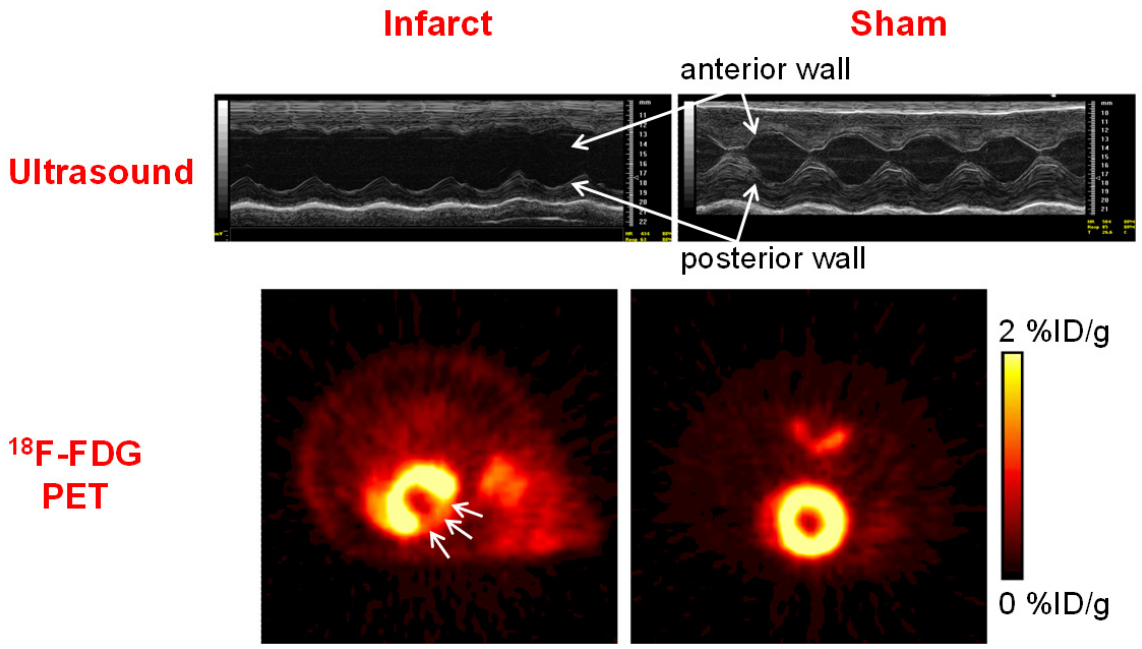

Figure 1. In echocardiogram of female rats on post-operative day 3, the signal from the posterior wall is visible in both the infarct and sham groups. However, there is no corresponding signal from the anterior wall in the infarcted heart which reflected the lack of movement. ^{18}F-FDG PET of the sham-operated heart demonstrated a complete circle, whereas a gap can be clearly seen (white arrows) in the infarcted heart. Both experiments confirmed the presence of myocardial infarction in the "infarct" group and intact heart in the "sham" group.

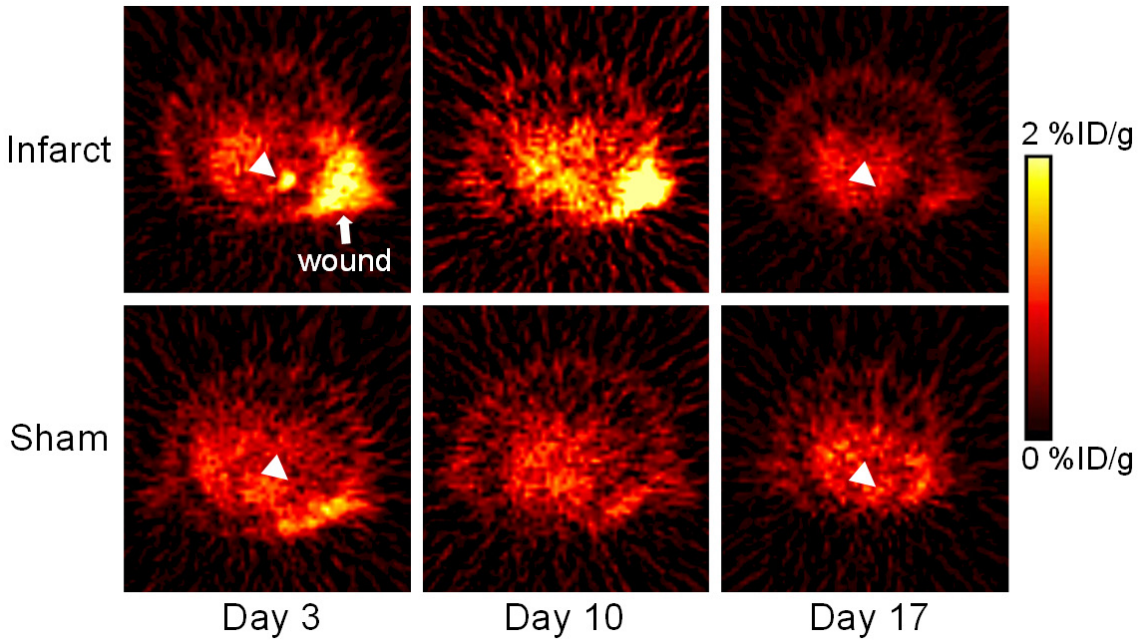

Figure 2. ^{64}Cu-NOTA-TRC105 PET images on days 3, 10 and 17 after surgery. Images were acquired at 48 h post-injection of the tracer and only transaxial images containing the heart are shown. The heart wall (with or without infarct) is indicated with white arrowheads. Tracer uptake in the intercostal incision (denoted as "wound") could also be visualized in some of the images. On day 17, neither the infarct zone nor the incision site showed prominent tracer uptake above the background level.

(VisualSonics, Toronto, Canada) on post-operative day 3. Non-invasive acquisition of two-dimensional B-mode and M-mode images was recorded on anesthetized rats (with 1% isoflu-

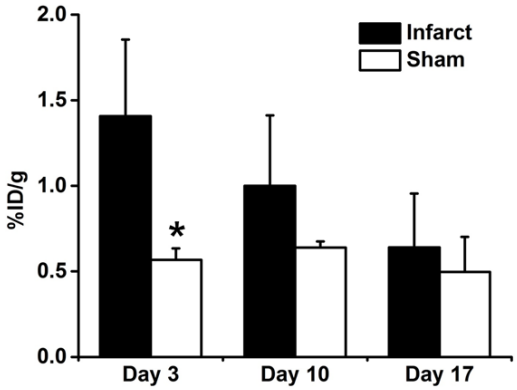

Figure 3. Quantitative PET data based in images obtained at 48 h post-injection of ^{64}Cu-NOTA-TRC105 on different days after surgery (n=3). *: P<0.05.

rane). Abnormal wall motion was noted in a long axis view to confirm MI. Ejection Fraction ((stroke volume/end-diastolic volume) × 100) was measured from a standard long axis view via calculations using VisualSonics software. ^{18}F-fluoro-2-deoxy-D-glucose (^{18}F-FDG) PET scans were also utilized to further confirm the presence of MI. One hour after each rat was injected with ~37 MBq of ^{18}F-FDG, a 20 min static scan was carried out with the mid thorax of the rat in the center of the scanner's field of view (FOV).

PET imaging

Serial PET imaging was performed on an Inveon microPET/microCT rodent model scanner (Siemens Medical Solutions USA, Inc.) as described previously [17, 21]. Animals were intravenously injected with 20-37 MBq of ^{64}Cu-NOTA-TRC105. Thirty-minute static PET scans were performed at various time points post-injection (p.i.), with the rats maintained under 2% isoflurane anesthesia and the mid thorax located in the center of the FOV. The images were reconstructed using a filtered back projection (FBP) algorithm, with no attenuation or scatter correction. Region-of-interest (ROI) analysis of each PET scan was performed using vendor software (Inveon Research Workplace [IRW]) on decay-corrected whole-body images as described previously [17, 21], to calculate the percentage injected dose per gram of tissue (%ID/g) values for the infarcted and non-infarcted cardiac muscle.

Histopathology

Frozen tissue slices of 5 μm thickness were fixed with cold acetone for 10 min for hematoxylin and eosin (H & E) and immunofluorescence (IF) staining. For IF staining, after rinsing with PBS and blocking with 10% donkey serum for 30 min at room temperature, the slices were incubated with a mixture of TRC105 (5 μg/mL) and rat anti-mouse CD31 antibody (BD biosciences, San Jose, CA) for 1 h at room temperature, and visualized using AlexaFluor488-labeled goat anti-human IgG (Invitrogen, Eugene, OR) and Cy3-labeled donkey anti-rat IgG (Jackson laboratories, West Grove, PA) respectively. All images were acquired with a Nikon Eclipse Ti microscope. Vascular density was calculated under 20 × magnification. The average values of the vessel counts from 3 different high power fields (hpf; 0.12 mm^2) were calculated.

Statistical analysis

Data were presented as mean ± SD. Differences between multiple groups were assessed with 1-way ANOVA followed by the Tukey's post hoc test for multiple comparisons. All *P* values were calculated with 2-tailed statistical tests. Differences were considered statistically significant when $P<0.05$. Data were analyzed with GraphPad software.

Results

^{64}Cu-labeling of TRC105

^{64}Cu-labeling, including final purification using size exclusion column chromatography, took 80 ± 10 min (n=5). The decay-corrected radiochemical yield was >85% based on 25 μg of NOTA-TRC105 per 37 MBq of ^{64}Cu, and the radiochemical purity was >98%. The specific activity of ^{64}Cu-NOTA-TRC105 was about 1.2 GBq/mg of protein, assuming complete recovery of NOTA-TRC105 after size exclusion column chromatography.

Characterization of MI in rats

On day 3 after MI, ultrasound was used to assess cardiovascular function and wall motion abnormalities (**Figure 1**). MI rats had an ejection fraction of 27 ± 11% (n=3), which is significantly lower than the average ejection fraction for normal rats under isoflurane anesthesia (~60% [22]). ^{18}F-FDG uptake was prominent and homogenous in the myocardial tissue in the sham group, whereas the infarcted myocardial tissue in the MI group had profoundly decreased uptake of ^{18}F-FDG (**Figure 1**). Taken

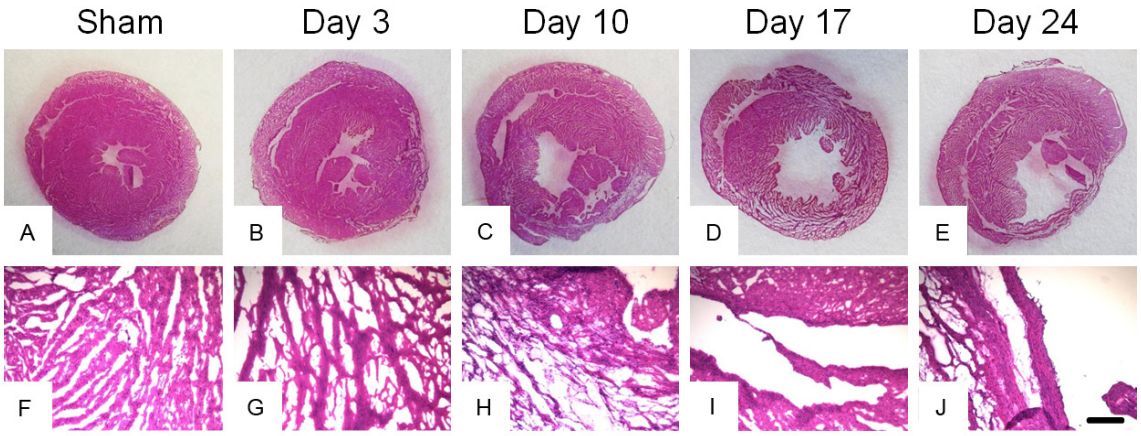

Figure 4. The upper row of images show the normal heart and the progressive changes in the infarcted heart on days 3, 10, 17, and 24 in lower magnification. The thickness of the myocardium is even all around the cardiac wall in normal heart (A). No significant thinning can be seen on day 3 (B), whereas a marked thinning in the infarcted anterolateral wall can be seen starting from day 10 (C). Thinning becomes more evident on day 17 (D) and finally the infarct zone is completely replaced by a thin fibrotic layer on day 24 (E). The bottom row shows the corresponding higher magnification images from the infract zone. Even though panel B shows little change on day 3, the higher magnification view shows the beginning of histological changes, characterized by the thinning of the myocardial fibrils (G) in comparison to normal heart (F). Disorganized and thinner myocardial fibrils are more evident on days 10, 17, and 24 (H-J). Scale bar: 200 μm.

together, both experiments confirmed the successful generation of MI after surgery.

PET imaging

^{64}Cu-NOTA-TRC105 PET was carried out on days 3, 10, and 17 following surgery to non-invasively monitor CD105 expression in the infarct zone (**Figure 2**). On the basis of our previous experience with in vivo PET imaging using TRC105-based agents to image CD105 expression on proliferating tumor vasculature [23], the time points of 4, 24, and 48 h p.i. were chosen for serial PET scans. At 4 h p.i., typically there was a relatively high level of blood radioactivity because of the long circulation half-life of the radiolabeled antibody. ^{64}Cu-NOTA-TRC105 uptake in the tissue of interest (e.g., tumor and ischemic tissue) typically plateaued between 24 and 48 h p.i. [20, 23].

In this study, since the ROI was in the rat heart, PET images at 4 h and 24 h p.i. were less informative due to high background signal in the blood pool. Therefore, ROI analysis was performed for PET data acquired at 48 h p.i., which showed minimal blood pool radioactivity and allowed for clear visualization of tracer uptake in the rat heart. ^{64}Cu-NOTA-TRC105 uptake in the infarct zone at 48 h p.i. was 1.41 ± 0.45, 1.00 ± 0.41, and 0.64 ± 0.31 %ID/g on days 3, 10, and 17 following surgery, respectively (n=3; **Figure 3**). These values were higher than that of the sham-operated rats (0.57 ± 0.07, 0.64 ± 0.04, and 0.50 ± 0.21 %ID/g on days 3, 10, and 17, respectively; n=3). On day 3, the difference was statistically significant between the two groups with $P<0.05$. Afterwards, the difference in tracer uptake was no longer statistically significant, although ^{64}Cu-NOTA-TRC105 uptake was higher in the MI group when compared to the sham group on post-operative day 10.

Histopathology

H & E staining indicated the progressive replacement of the infarcted myocardium with fibrotic tissue, with the whole sections of the rat heart shown in **Figure 4A-E** and the higher magnification images shown in **Figure 4F-J**. CD31/CD105 co-staining images of the heart were shown in **Figure 5**. An increased expression of CD105 was observed on days 3 and 10 after the surgery. The highest density of CD105-positive vessels was observed on post-operative day 3 (17.6 ± 2.5 vessels/hpf; n=3), followed by day 10 (14.0 ± 3.6 vessels/hpf; n=3). The average number of CD105-positive vessels dropped to 4.6 ± 0.6 vessels/hpf (n=3) on day 17. The difference in CD105-positive vessel density between post-operative days 3 and 10 was not statistically significant, while the difference between day 3 (or day 10) and day 17 was sta-

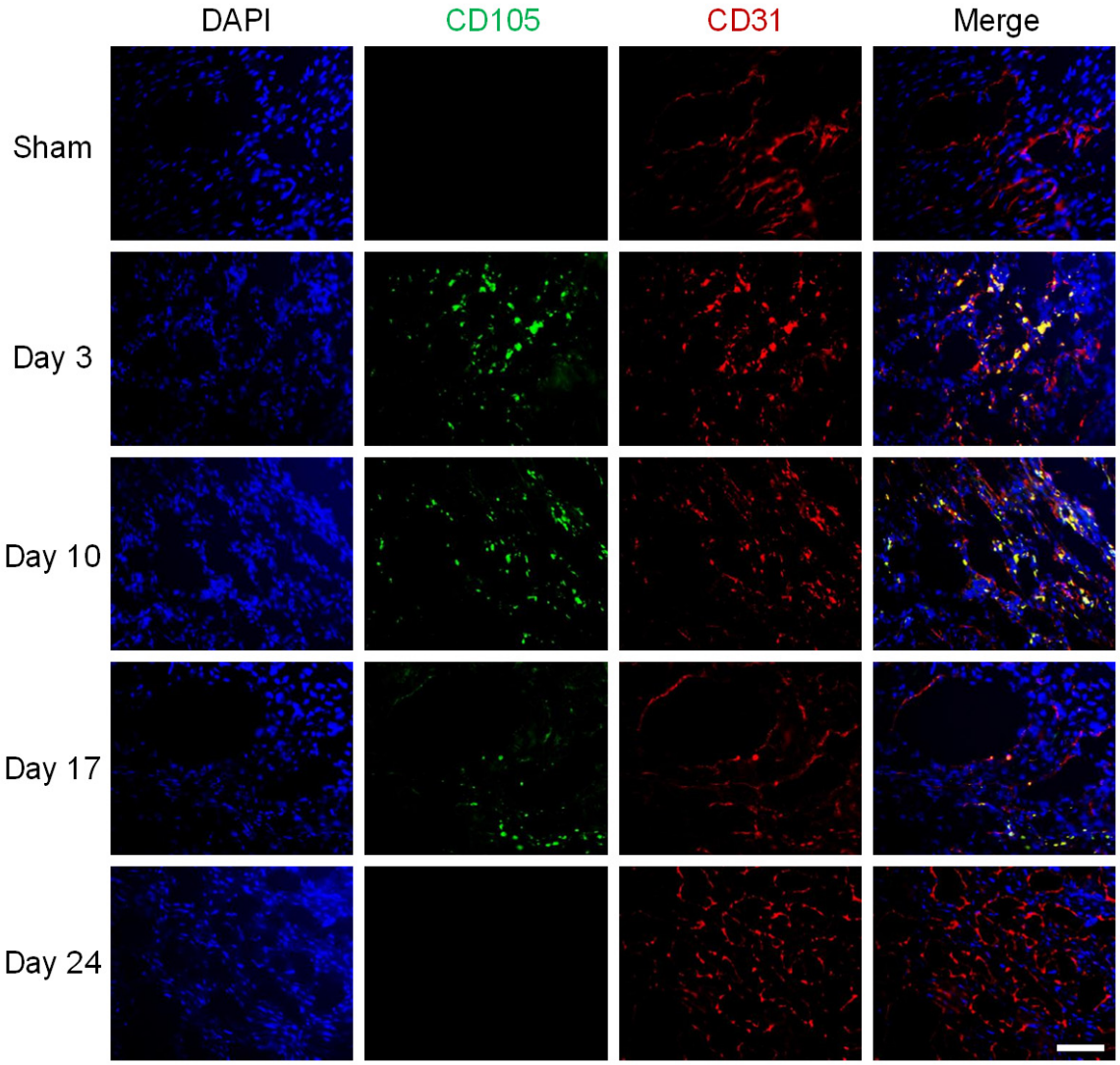

Figure 5. Representative images from CD31/CD105 co-staining of sham-operated and infarcted heart. DAPI staining was used to indicate the nuclei and merged images are also shown. Scale bar: 100 μm.

tistically significant ($P<0.05$). No significant CD105 staining was observed in the sham group, which corroborated the in vivo findings.

Discussion

In this study, we investigated the progress of post-MI angiogenesis via PET imaging of CD105 expression in a rat model of MI. Traditional cardiac imaging is based on the detection of anatomic and physiologic changes in the heart, such as changes in blood flow or contractile function. Because of high throughput and wide availability, echocardiography remains the workhorse in the field of cardiac imaging [2]. In the case of chronic ischemic injury, the extent of infarct may be visualized accurately with newer generation ultrasound systems. However, in the case of acute ischemic injury, simple assessment of the abnormalities of wall motion can result in significant overestimation of the infarction size [24]. Molecular imaging techniques such as PET can allow in vivo studies of biological pathways of various cardiovascular diseases, including altered energy metabolism, inflammation, apoptosis, thrombosis, and angiogenesis, thus enabling early diagnosis and improved therapeutic approaches [25]. PET imaging may provide invaluable in vivo information with regard to the pathophysiology of MI and, because of its non-invasive nature, may be readily applied to human subjects.

The biological changes following MI can be assessed by the evaluation of regional myocar-

dial perfusion, function, and metabolism via various molecular imaging techniques [3, 26]. PET tracers used for the evaluation of myocardial blood flow typically include ^{13}N-ammonia, ^{82}Rb, and ^{15}O-H_2O [27-30]. However, the short decay half-lives of these radiotracers limit their widespread clinical use, because of the need for an on-site cyclotron or generator. ^{13}N-NH_3 has a relatively long decay half-life of ten minutes, high myocardium extraction, and reduced persistence in the blood pool, which make it more amenable than ^{82}Rb and ^{15}O-H_2O for preclinical studies [28]. ^{18}F-FDG can measure the changes in glucose metabolism and it is the most widely used PET tracer in the clinic [31-33]. The uptake of ^{18}F-FDG by myocardium provides an established clinical method to measure tissue viability in patients with MI. When compared to other PET tracers, ^{18}F-FDG is more readily available at most PET centers and allows the acquisition of images with good resolution [26, 31].

However, none of these abovementioned tracers demonstrate biological changes occurring in the actual infarct zone. Therefore, many other PET tracers have been developed to target ischemia induced-angiogenesis occurring in the infarct zone, such as those that target the integrins (with radiolabeled RGD peptides) or VEGFR (with radiolabeled VEGF protein) [4, 10, 13, 34, 35]. In this work, we have shown that CD105 is another relevant and valid target for investigation of post-MI angiogenesis, using our previously validated ^{64}Cu-NOTA-TRC105 as the PET tracer [19, 20]. When compared with the literature reports mentioned above, PET image quality and ^{64}Cu-NOTA-TRC105 uptake in the infarct zone were comparable to the other PET tracers. In the clinic, there is an urgent need for molecular imaging strategies that can provide clinicians with biological information for the diagnosis and treatment of ischemic heart disease. Although molecular imaging techniques have advanced dramatically over the last decade in preclinical models, much future effort needs to be devoted to clinical translation.

The limitations of our study are primarily related to the animal model. The arterial territories of rat coronary arteries are quite different from human coronary arteries. These differences may result in different zones of infarction in rats when compared to humans, even though the same artery is occluded [26]. Another shortcoming is the acuteness of the myocardial ischemia in our rat model, unlike human MI which may be associated with a chronic ischemic process. The progress of post-MI remodeling may differ between humans and rats because of differences in pathogenesis. Another issue is that permanent ligation of the LAD artery was adopted in our rat model of MI, whereas in the clinic blood flow in MI patients would generally be re-established. The lack of blood flow in the LAD artery after surgery could significantly affect tracer uptake in the infarct area. Of note, the skin incision was placed as far away as possible from the heart, which allowed us to partly avoid the background signal from the skin incision during PET imaging. Nonetheless, the incision on the intercostal muscles produced a strong background signal that could clearly be seen in PET (**Figure 2**), since wound healing involves angiogenesis and CD105 is most likely also overexpressed during this process, which may obscure the specific signal from the infarct region to a certain extent. This may be partly responsible for the relatively large error bars of tracer uptake in the MI group.

Conclusion

Herein we report the use of ^{64}Cu-NOTA-TRC105 for non-invasive assessment of angiogenesis following acute MI in a rat model. Echocardiography and ^{18}F-FDG PET was used to confirm the successful induction of MI in female rats, which exhibited elevated uptake of ^{64}Cu-NOTA-TRC105 in the infarct zone (significantly higher than that of the sham group on post-operative day 3). Histopathology confirmed increased CD105 expression following MI, indicating that CD105 is a viable target for imaging and therapeutic intervention of MI. Overall, this study suggested that PET imaging of CD105 can be a useful tool for MI-related research, which may improve MI patient management in the future upon clinical translation of the optimized PET tracers.

Acknowledgements

This work is supported, in part, by the University of Wisconsin - Madison, the National Institutes of Health (NIBIB/NCI 1R01CA169365 and 5T32GM08349), the Department of Defense (W81XWH-11-1-0644), the American Cancer Society (125246-RSG-13-099-01-CCE), and

the National Science Foundation (DGE-125-6259).

Disclosure of conflict of interest

CPT is an employee of TRACON Pharmaceuticals, Inc. The other authors declare no conflicts of interest.

Address correspondence to: Dr. Weibo Cai, Departments of Radiology and Medical Physics, School of Medicine and Public Health, University of Wisconsin - Madison, Room 7137, 1111 Highland Ave, Madison, WI 53705-2275, USA. Tel: 1-608-262-1749; Fax: 1-608-265-0614; E-mail: wcai@uwhealth.org

References

[1] Lloyd-Jones D, Adams R, Carnethon M, De Simone G, Ferguson TB, Flegal K, Ford E, Furie K, Go A, Greenlund K, Haase N, Hailpern S, Ho M, Howard V, Kissela B, Kittner S, Lackland D, Lisabeth L, Marelli A, McDermott M, Meigs J, Mozaffarian D, Nichol G, O'Donnell C, Roger V, Rosamond W, Sacco R, Sorlie P, Stafford R, Steinberger J, Thom T, Wasserthiel-Smoller S, Wong N, Wylie-Rosett J, Hong Y; American Heart Association Statistics Committee and Stroke Statistics Subcommittee. Heart disease and stroke statistics--2009 update: a report from the American Heart Association Statistics Committee and Stroke Statistics Subcommittee. Circulation 2009; 119: 480-486.

[2] Kramer CM, Sinusas AJ, Sosnovik DE, French BA and Bengel FM. Multimodality imaging of myocardial injury and remodeling. J Nucl Med 2010; 51 Suppl 1: 107S-121S.

[3] Dobrucki LW and Sinusas AJ. Imaging angiogenesis. Curr Opin Biotechnol 2007; 18: 90-96.

[4] Menichetti L, Kusmic C, Panetta D, Arosio D, Petroni D, Matteucci M, Salvadori PA, Casagrande C, L'Abbate A and Manzoni L. MicroPET/CT imaging of alphabeta integrin via a novel Ga-NOTA-RGD peptidomimetic conjugate in rat myocardial infarction. Eur J Nucl Med Mol Imaging 2013; 40: 1265-1274.

[5] James ML and Gambhir SS. A molecular imaging primer: modalities, imaging agents, and applications. Physiol Rev 2012; 92: 897-965.

[6] Nolting DD, Nickels ML, Guo N and Pham W. Molecular imaging probe development: a chemistry perspective. Am J Nucl Med Mol Imaging 2012; 2: 273-306.

[7] Sherif HM, Saraste A, Weidl E, Weber AW, Higuchi T, Reder S, Poethko T, Henriksen G, Casebier D, Robinson S, Wester HJ, Nekolla SG and Schwaiger M. Evaluation of a novel ^{18}F-labeled positron-emission tomography perfusion tracer for the assessment of myocardial infarct size in rats. Circ Cardiovasc Imaging 2009; 2: 77-84.

[8] Cai W and Chen X. Multimodality molecular imaging of tumor angiogenesis. J Nucl Med 2008; 49 Suppl 2: 113S-128S.

[9] Cai W, Niu G and Chen X. Imaging of integrins as biomarkers for tumor angiogenesis. Curr Pharm Des 2008; 14: 2943-2973.

[10] Rodriguez-Porcel M, Cai W, Gheysens O, Willmann JK, Chen K, Wang H, Chen IY, He L, Wu JC, Li ZB, Mohamedali KA, Kim S, Rosenblum MG, Chen X and Gambhir SS. Imaging of VEGF receptor in a rat myocardial infarction model using PET. J Nucl Med 2008; 49: 667-673.

[11] Meoli DF, Sadeghi MM, Krassilnikova S, Bourke BN, Giordano FJ, Dione DP, Su H, Edwards DS, Liu S, Harris TD, Madri JA, Zaret BL and Sinusas AJ. Noninvasive imaging of myocardial angiogenesis following experimental myocardial infarction. J Clin Invest 2004; 113: 1684-1691.

[12] Lu E, Wagner WR, Schellenberger U, Abraham JA, Klibanov AL, Woulfe SR, Csikari MM, Fischer D, Schreiner GF, Brandenburger GH and Villanueva FS. Targeted in vivo labeling of receptors for vascular endothelial growth factor: approach to identification of ischemic tissue. Circulation 2003; 108: 97-103.

[13] Gao H, Lang L, Guo N, Cao F, Quan Q, Hu S, Kiesewetter DO, Niu G and Chen X. PET imaging of angiogenesis after myocardial infarction/reperfusion using a one-step labeled integrin-targeted tracer ^{18}F-AlF-NOTA-PRGD2. Eur J Nucl Med Mol Imaging 2012; 39: 683-692.

[14] Hong H, Zhang Y, Orbay H, Valdovinos HF, Nayak TR, Bean J, Theuer CP, Barnhart TE and Cai W. Positron emission tomography imaging of tumor angiogenesis with a $^{61/64}$Cu-labeled F(ab')$_2$ antibody fragment. Mol Pharm 2013; 10: 709-716.

[15] Zhang Y, Hong H, Nayak TR, Valdovinos HF, Myklejord DV, Theuer CP, Barnhart TE and Cai W. Imaging tumor angiogenesis in breast cancer experimental lung metastasis with positron emission tomography, near-infrared fluorescence, and bioluminescence. Angiogenesis 2013; 16: 663-674.

[16] Zhang Y, Hong H, Orbay H, Valdovinos HF, Nayak TR, Theuer CP, Barnhart TE and Cai W. PET imaging of CD105/endoglin expression with a $^{61/64}$Cu-labeled Fab antibody fragment. Eur J Nucl Med Mol Imaging 2013; 40: 759-767.

[17] Zhang Y, Hong H, Severin GW, Engle JW, Yang Y, Goel S, Nathanson AJ, Liu G, Nickles RJ, Leigh BR, Barnhart TE and Cai W. ImmunoPET and near-infrared fluorescence imaging of CD105

expression using a monoclonal antibody dual-labeled with ^{89}Zr and IRDye 800CW. Am J Transl Res 2012; 4: 333-346.

[18] Rosen LS, Hurwitz HI, Wong MK, Goldman J, Mendelson DS, Figg WD, Spencer S, Adams BJ, Alvarez D, Seon BK, Theuer CP, Leigh BR and Gordon MS. A phase I first-in-human study of TRC105 (Anti-Endoglin Antibody) in patients with advanced cancer. Clin Cancer Res 2012; 18: 4820-4829.

[19] Zhang Y, Hong H, Engle JW, Bean J, Yang Y, Leigh BR, Barnhart TE and Cai W. Positron emission tomography imaging of CD105 expression with a ^{64}Cu-labeled monoclonal antibody: NOTA is superior to DOTA. PLoS One 2011; 6: e28005.

[20] Orbay H, Zhang Y, Hong H, Hacker TA, Valdovinos HF, Zagzebski JA, Theuer CP, Barnhart TE and Cai W. Positron Emission Tomography Imaging of Angiogenesis in a Murine Hindlimb Ischemia Model with ^{64}Cu-Labeled TRC105. Mol Pharm 2013; 10: 2749-2756.

[21] Zhang Y, Hong H, Engle JW, Yang Y, Barnhart TE and Cai W. Positron Emission Tomography and Near-Infrared Fluorescence Imaging of Vascular Endothelial Growth Factor with Dual-Labeled Bevacizumab. Am J Nucl Med Mol Imaging 2012; 2: 1-13.

[22] Watson LE, Sheth M, Denyer RF and Dostal DE. Baseline echocardiographic values for adult male rats. J Am Soc Echocardiogr 2004; 17: 161-167.

[23] Hong H, Yang Y, Zhang Y, Engle JW, Barnhart TE, Nickles RJ, Leigh BR and Cai W. Positron emission tomography imaging of CD105 expression during tumor angiogenesis. Eur J Nucl Med Mol Imaging 2011; 38: 1335-1343.

[24] Thomas D, Bal H, Arkles J, Horowitz J, Araujo L, Acton PD and Ferrari VA. Noninvasive assessment of myocardial viability in a small animal model: comparison of MRI, SPECT, and PET. Magn Reson Med 2008; 59: 252-259.

[25] Sinusas AJ. Molecular imaging in nuclear cardiology: translating research concepts into clinical applications. Q J Nucl Med Mol Imaging 2010; 54: 230-240.

[26] Gargiulo S, Greco A, Gramanzini M, Petretta MP, Ferro A, Larobina M, Panico M, Brunetti A and Cuocolo A. PET/CT imaging in mouse models of myocardial ischemia. J Biomed Biotechnol 2012; 2012: 541872.

[27] Kudo T, Fukuchi K, Annala AJ, Chatziioannou AF, Allada V, Dahlbom M, Tai YC, Inubushi M, Huang SC, Cherry SR, Phelps ME and Schelbert HR. Noninvasive measurement of myocardial activity concentrations and perfusion defect sizes in rats with a new small-animal positron emission tomograph. Circulation 2002; 106: 118-123.

[28] Inubushi M, Jordan MC, Roos KP, Ross RS, Chatziioannou AF, Stout DB, Dahlbom M and Schelbert HR. Nitrogen-13 ammonia cardiac positron emission tomography in mice: effects of clonidine-induced changes in cardiac work on myocardial perfusion. Eur J Nucl Med Mol Imaging 2004; 31: 110-116.

[29] Yoshinaga K, Chow BJ, Williams K, Chen L, deKemp RA, Garrard L, Lok-Tin Szeto A, Aung M, Davies RA, Ruddy TD and Beanlands RS. What is the prognostic value of myocardial perfusion imaging using rubidium-82 positron emission tomography? J Am Coll Cardiol 2006; 48: 1029-1039.

[30] Yamamoto Y, de Silva R, Rhodes CG, Araujo LI, Iida H, Rechavia E, Nihoyannopoulos P, Hackett D, Galassi AR, Taylor CJ and et al. A new strategy for the assessment of viable myocardium and regional myocardial blood flow using 150-water and dynamic positron emission tomography. Circulation 1992; 86: 167-178.

[31] Ghesani M, Depuey EG and Rozanski A. Role of F-18 FDG positron emission tomography (PET) in the assessment of myocardial viability. Echocardiography 2005; 22: 165-177.

[32] Alauddin MM. Positron emission tomography (PET) imaging with ^{18}F-based radiotracers. Am J Nucl Med Mol Imaging 2012; 2: 55-76.

[33] Rischpler C, Nekolla SG and Beer AJ. PET/MR imaging of atherosclerosis: initial experience and outlook. Am J Nucl Med Mol Imaging 2013; 3: 393-396.

[34] Higuchi T, Bengel FM, Seidl S, Watzlowik P, Kessler H, Hegenloh R, Reder S, Nekolla SG, Wester HJ and Schwaiger M. Assessment of alphavbeta3 integrin expression after myocardial infarction by positron emission tomography. Cardiovasc Res 2008; 78: 395-403.

[35] Laitinen I, Notni J, Pohle K, Rudelius M, Farrell E, Nekolla SG, Henriksen G, Neubauer S, Kessler H, Wester HJ and Schwaiger M. Comparison of cyclic RGD peptides for alphavbeta3 integrin detection in a rat model of myocardial infarction. EJNMMI Res 2013; 3: 38.